

# Large-scale evaluation of ANTs and FreeSurfer cortical thickness measurements<sup>☆</sup>

**Q1** Nicholas J. Tustison <sup>a,\*</sup>, Philip A. Cook <sup>b</sup>, Arno Klein <sup>c</sup>, Gang Song <sup>b</sup>, Sandhitsu R. Das <sup>b</sup>, Jeffrey T. Duda <sup>b</sup>,  
**Q4** Benjamin M. Kandel <sup>b</sup>, Niels van Strien <sup>c</sup>, James R. Stone <sup>a</sup>, James C. Gee <sup>b</sup>, Brian B. Avants <sup>b,d</sup>

**Q5** <sup>a</sup> Department of Radiology and Medical Imaging, University of Virginia, Charlottesville, VA, USA

**6** <sup>b</sup> Penn Image Computing and Science Laboratory, University of Pennsylvania, Philadelphia, PA, USA

**7** <sup>c</sup> Sage Bionetworks, Seattle, WA, USA

**8** <sup>d</sup> Department of Circulation and Medical Imaging, Norwegian University of Science and Technology, Trondheim, Norway

## ARTICLE INFO

### Article history:

Accepted 15 May 2014

Available online xxxx

### Keywords:

Advanced normalization tool

Age prediction

MRI

Gender prediction

Open science

Scientific reproducibility

## ABSTRACT

Many studies of the human brain have explored the relationship between cortical thickness and cognition, phenotype, or disease. Due to the subjectivity and time requirements in manual measurement of cortical thickness, scientists have relied on robust software tools for automation which facilitate the testing and refinement of neuroscientific hypotheses. The most widely used tool for cortical thickness studies is the publicly available, surface-based FreeSurfer package. Critical to the adoption of such tools is a demonstration of their reproducibility, validity, and the documentation of specific implementations that are robust across large, diverse imaging datasets. To this end, we have developed the automated, volume-based Advanced Normalization Tools (ANTs) cortical thickness pipeline comprising well-vetted components such as SyGN (multivariate template construction), SyN (image registration), N4 (bias correction), Atropos (*n*-tissue segmentation), and DiReCT (cortical thickness estimation). In this work, we have conducted the largest evaluation of automated cortical thickness measures in publicly available data, comparing FreeSurfer and ANTs measures computed on 1205 images from four open data sets (IXI, MMR, NKI, and OASIS), with parcellation based on the recently proposed Desikan-Killiany-Tourville (DKT) cortical labeling protocol. We found good scan-rescan repeatability with both FreeSurfer and ANTs measures. Given that such assessments of precision do not necessarily reflect accuracy or an ability to make statistical inferences, we further tested the neurobiological validity of these approaches by evaluating thickness-based prediction of age and gender. ANTs is shown to have a higher predictive performance than FreeSurfer for both of these measures. In promotion of open science, we make all of our scripts, data, and results publicly available which complements the use of open image data sets and the open source availability of the proposed ANTs cortical thickness pipeline.

© 2014 Elsevier Inc. All rights reserved.

39

40

42

## Introduction

**Q6** Magnetic resonance imaging-based structural analysis of the human brain plays a fundamental role in identifying the relationship between cortical morphology, disease, and cognition. Such research has yielded insight concerning cortical variability and its developmental correlates including those associated with normal aging (Walhovd et al., 2013) and gender differences (Luders et al., 2006). Conditional abnormalities from Alzheimer's disease and frontotemporal dementia (Dickerson et al., 2009; Du et al., 2007) to Parkinson's (Jubault et al., 2011) and Huntington's disease (Rosas et al., 2005) also demonstrate sensitivity to cortical thickness assessments. Additional explorations have included

such topics of interest as autism (Chung et al., 2005), athletic ability (Wei et al., 2011), male-to-female transsexuality (Luders et al., 2012), obesity (Raji et al., 2010), and Tetris-playing ability in female adolescents (Haier et al., 2009). Although these findings are subject to debate and interpretation (Gernsbacher, 2007), the availability of quantitative computational methods for extracting cortical thickness measures has proven invaluable for developing and refining fundamental neuroscience hypotheses.

Computational methods for analyzing the cortex may be broadly characterized as surface mesh-based or volumetric (Clarkson et al., 2011; Scott et al., 2009). Representative of the former is the FreeSurfer cortical modeling software package (Dale et al., 1999; Fischl and Dale, 2000; Fischl et al., 1999, 2002, 2004) which owes its popularity to public availability, excellent documentation, good performance, and integration with other toolkits, such as the extensive FMRIB software library (Smith et al., 2004). Similar to other surface-based cortical thickness estimation approaches (e.g., Davatzikos and Bryan, 1996; Kim et al., 2005;

<sup>☆</sup> Partial support was provided by the Defense Health Program through the U.S. Army Medical Research Acquisition Activity, Grant Number W81XWH-09-2-0055.

\* Corresponding author at: PO Box 801339, Charlottesville, VA 22908, USA.

E-mail address: ntustison@virginia.edu (N.J. Tustison).

t1.1  
Q3 1.2

**Table 1**  
The 31 cortical labels (per hemisphere) of the DKT atlas.

|                              |                                  |
|------------------------------|----------------------------------|
| 1) Caudal anterior cingulate | 17) Pars orbitalis               |
| 2) Caudal middle frontal     | 18) Pars triangularis            |
| 3) Cuneus                    | 19) Pericalcarine                |
| 4) Entorhinal                | 20) Postcentral                  |
| 5) Fusiform                  | 21) Posterior cingulate          |
| 6) Inferior parietal         | 22) Precentral                   |
| 7) Inferior temporal         | 23) Precuneus                    |
| 8) Isthmus cingulate         | 24) Rosterior anterior cingulate |
| 9) Lateral occipital         | 25) Rostral middle frontal       |
| 10) Lateral orbitofrontal    | 26) Superior frontal             |
| 11) Lingual                  | 27) Superior parietal            |
| 12) Medial orbitofrontal     | 28) Superior temporal            |
| 13) Middle temporal          | 29) Supramarginal                |
| 14) Parahippocampal          | 30) Transverse temporal          |
| 15) Paracentral              | 31) Insula                       |
| 16) Pars opercularis         |                                  |

# Processing calls for subject IXI002-Guys-0828-T1

```
# ANTs
antsCorticalThickness.sh \
-a IXI/T1/IXI002-Guys-0828-T1.nii.gz \
-e IXI/template/T_template0.nii.gz \
-m IXI/template/T_template0ProbabilityMask.nii.gz \
-f IXI/template/T_template0ExtractionMask.nii.gz \
-p IXI/template/Priors/priors%d.nii.gz \
-o IXI/ANTSResults/IXI002-Guys-0828-
```

```
# FreeSurfer
recon-all \
-i IXI/T1/IXI002-Guys-0828-T1.nii.gz \
-s IXI002-Guys-0828 \
-sd IXI/FreeSurferResults/ \
-all
```

**Listing 1.** Analogous ANTs and FreeSurfer command line calls for a single IXI subject in the evaluation study.

MacDonald et al., 2000; Magnotta et al., 1999), the outer cortical and gray/white matter surfaces from individual subject MR data are modeled with polygonal meshes which are then used to determine local cortical thickness values based on a specified correspondence between the surface models.

Image volumetric (or meshless) techniques vary both in their algorithms as well as in the underlying definitions of cortical thickness. An early, foundational technique is the method of Jones et al. (2000) in which the inner and outer surface geometry is used to determine the solution to Laplace's equation where thickness is measured by integrating along the tangents of the resulting field lines spanning the boundary surfaces. Subsequent contributions improved upon the original formulation. For example, in Yezzi and Prince (2003), a Eulerian partial differential equation approach was proposed to facilitate the computation of correspondence paths. Extending the surface-based work of MacDonald et al. (2000), the hybrid approach of Kim et al. (2005) uses the discrete Laplacian field to deform the white matter surface mesh towards the

outer cortical surface. Other volumetric algorithms employ coupled level sets (Zeng et al., 1999), model-free intelligent search strategies either normal to the gray–white matter interface (Scott et al., 2009), or using a min–max rule (Vachet et al., 2011). Most relevant to this work is the DiReCT (Diffeomorphic Registration-based Cortical Thickness) algorithm proposed in Das et al. (2009) where generated diffeomorphic mappings between the gray/white matter and exterior cortical surfaces are used to propagate thickness values through the cortical gray matter.

The general lack of availability of published algorithms (Kovacevic, 2006) (not to mention critical preprocessing components) is a strong deterrent to the use or evaluation of these algorithms by external researchers. For example, one recent evaluation study (Clarkson et al., 2011) compared FreeSurfer (a surface-based method) with two volumetric methods, viz., Das et al. (2009) and Jones et al. (2000). Whereas the entire FreeSurfer processing pipeline has been made publicly available, refined by the original authors and other contributors, and described in

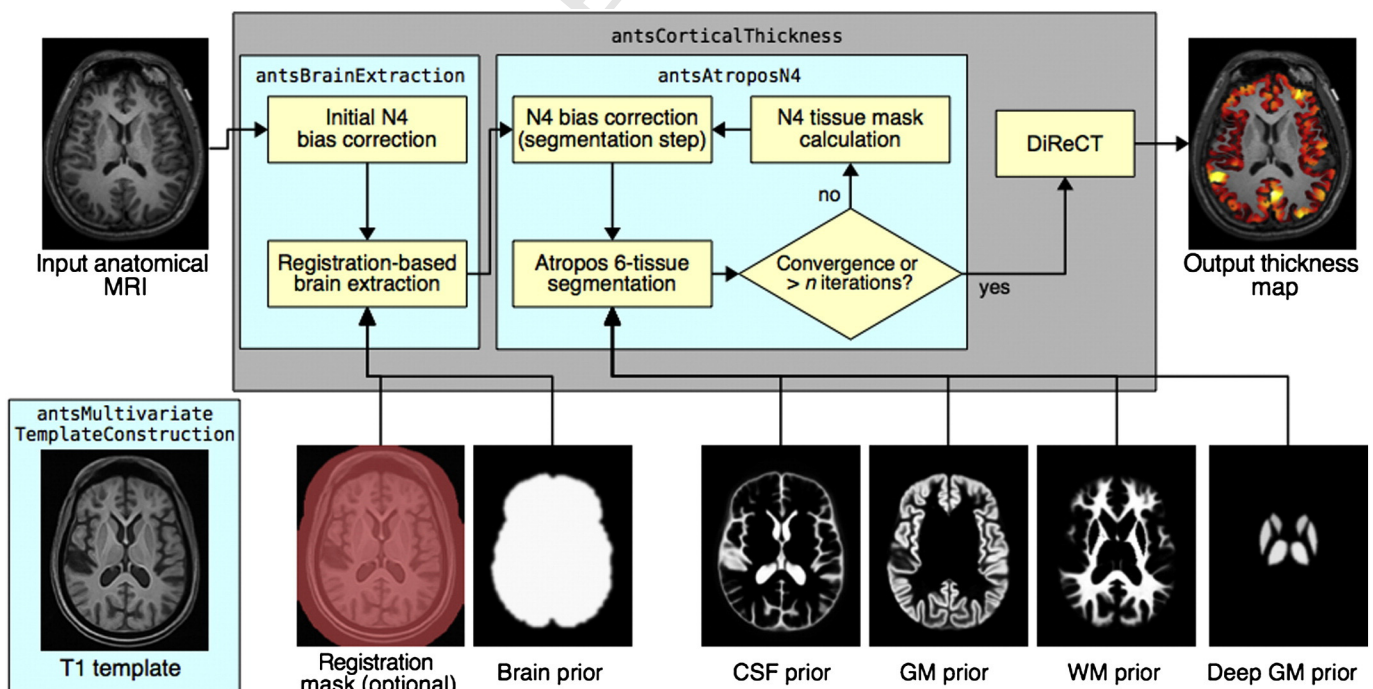


**Fig. 1.** Illustration of the main components of the ANTs processing workflow containing all elements for determining cortical thickness. We also included the domain of operations for the selected scripts. Not shown are the probability maps for the brain stem and cerebellum priors. All template-based prior probability maps are generated prior to pipeline processing of each individual subject.

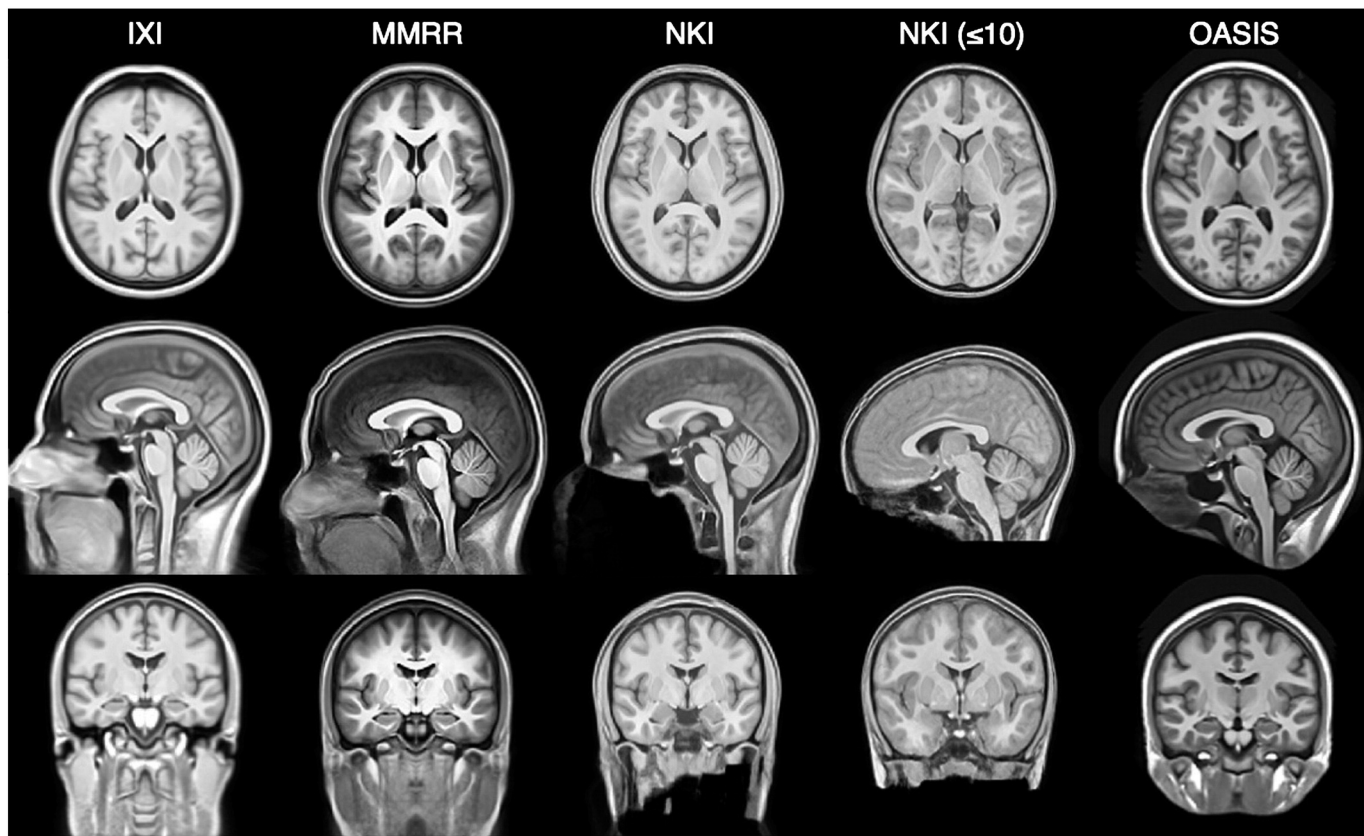


**Fig. 2.** Population-specific templates for each of the four public data sets used for cortical thickness estimation. The benefit of using such population-specific templates is obvious when one sees the variability in acquisition and data preparation (e.g., defacing protocols).

great detail (specifically in terms of suggested parameters), both volumetric methods were implemented and run by the authors of the evaluation (not by the algorithm developers) using unspecified parameters with relatively small, private data sets, making the comparisons less than ideal (see Tustison et al., 2013 for further discussion concerning the issue of instrumentation bias and scientific reproducibility in the use and evaluation of software). Further complicating such comparisons is the potential for bias, such as interpolation artifacts when converting surface to volume data or vice versa (Klein et al., 2010).

We provide below a brief description of our proposed pipeline, which produces a volumetric cortical thickness map from an individual subject's T1-weighted MRI. Additionally, we note that it is freely available as part of the Advanced Normalization Tools (ANTs) software package. This includes all the necessary preprocessing steps consisting of well-vetted, previously published algorithms for bias correction (Tustison et al., 2010), brain extraction (Avants et al., 2010a), *n*-tissue segmentation (Avants et al., 2011b), template construction (Avants et al., 2010b), and image normalization (Avants et al., 2011a). More importantly, we provide explicit coordination among these components within a set of well-documented shell scripts which are also available in the ANTs repository where parameters have been tuned by ANTs developers (N.T. and B.A.).

Here we demonstrate the use of the described framework in processing 1205 publicly available, T1-weighted brain MR images drawn from four well-known data sets. For comparative evaluation we also process the same data using the standard FreeSurfer cortical thickness processing protocol. Similar to previous work (e.g., Clarkson et al., 2011), we are able to report repeatability assessments for both frameworks using subsets of the data with repeated acquisitions. However, repeatability (or, more generally, *precision*) is not conceptually equivalent to *accuracy* and, thus, does not provide a complete perspective for the determination of measurement quality. Although FreeSurfer

validation has included histological (Rosas et al., 2002) and image-drawn (Kuperberg et al., 2003) comparisons, such manual assessments were extremely limited in terms of number of subjects and the number of cortical regions. In addition, there was no mention in these studies of the number of human observers making these measurements or discussion of quality assurance. Alternatively, without ground truth, other forms of evidence can be adduced (e.g., Bouix et al., 2007) in making comparative inferences. In this work we use demographic-based assessments (based on well-studied relationships between cortical thickness and age/gender) to show that ANTs outperforms FreeSurfer-based thickness estimation for these data in terms of prediction.

## Methods and materials

### Public data resources

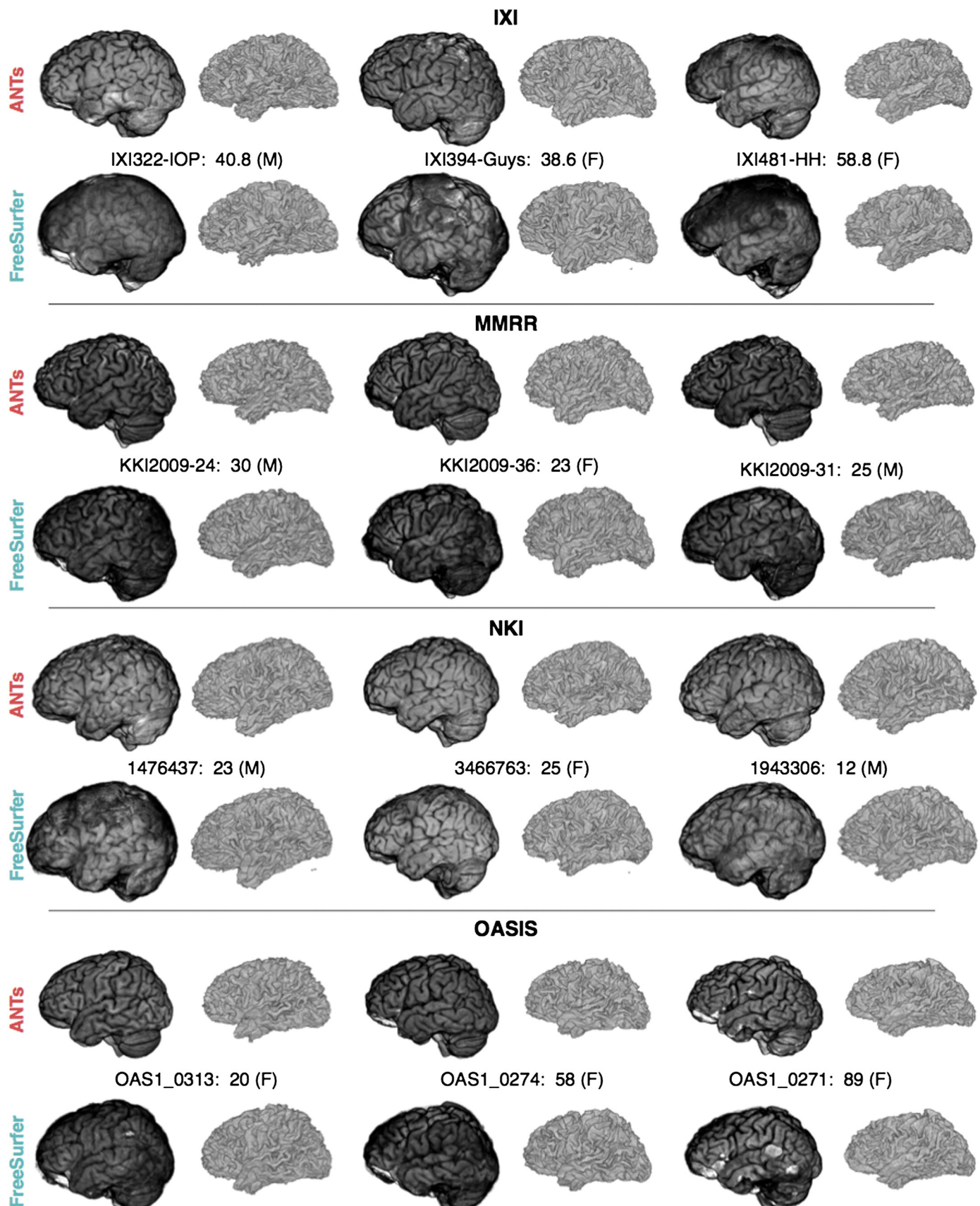
A comparative evaluation between FreeSurfer and ANTs was run on four publicly available data sets: IXI, MMRR, NKI, and OASIS. In addition to these data, we used a subset of the MindBoggle-101 data labeled using the Desikan-Killiany-Tourville (DKT) protocol (Klein and Tourville, 2012) to define the regions of interest (ROI) in the analysis. This latter data set was not included in the thickness analysis. All five data sets are described below.

### Public data for thickness estimation evaluation

Diverse and publicly available data sets collected from multiple sites with a mixture of 3 T and 1.5 T T1-weighted brain images were analyzed using the ANTs and FreeSurfer pipelines. Subjects in this data set span the age range from 4 to 96 years old. This strategy tested robustness to variation in head position, brain shape, defacing, image contrast, inhomogeneity, imaging artifacts, field strength, and the broad variation in extracerebral tissue. Failure can occur in initial

166 brain extraction, segmentation, registration, or bias correction, any  
 167 of which can lead to an inaccurate cortical thickness measurement.  
 168 In total, we processed 1205 T1-weighted images from four

169 different public data sets to obtain cortical thickness values for  
 170 both cortical thickness analysis software. Below we describe the  
 171 four data sets.



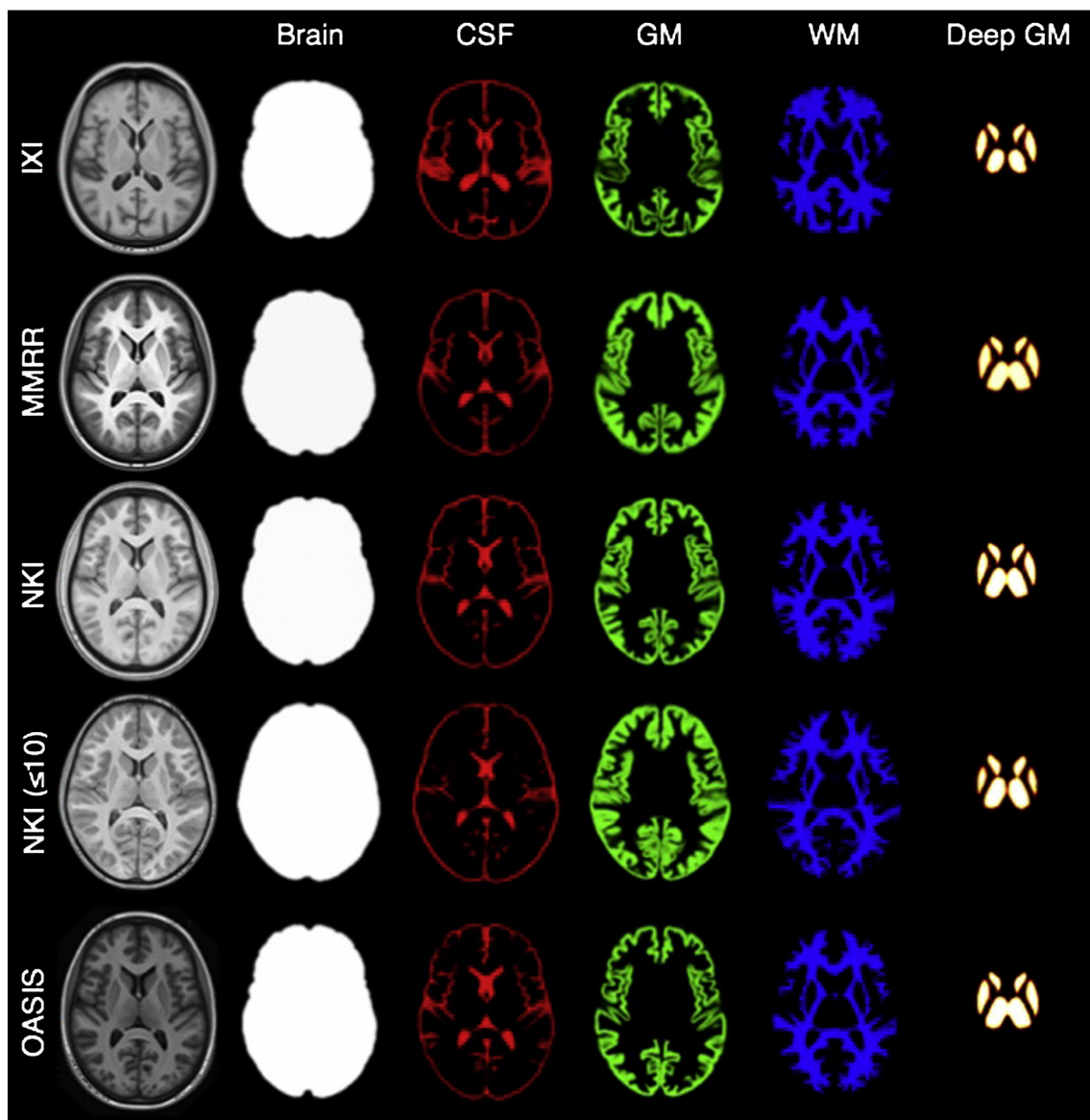


**Fig. 4.** Axial slices from each of the five T1 templates including the corresponding probability masks used for brain extraction and brain tissue segmentation. Not shown are the prior probability maps for brain stem and cerebellum regions.

**Q8** **IXI.** Initially, we processed 581 T1-weighted images from the IXI data  
173 set, but only 563 subjects (313 females, 250 males) were included in  
174 the post-processing analysis due to missing demographic information,  
175 which would have prevented an accurate estimate of the age at the  
176 time of image acquisition. These data were imaged at three sites with  
177 several modalities acquired (T1-weighted, T2-weighted, proton density,  
178 magnetic resonance angiography, and diffusion tensor imaging). The  
179 database also includes demographic information such as date of birth,  
180 date of scan, weight, height, ethnicity, occupation category, educational  
181 level, and marital status.

**MMRR.** The Multi-Modal MRI Reproducibility Resource (MMRR) data set, was originally described in Landman et al. (2011) consisting of 21 subjects (10 females, 11 males) and features a rich set of modalities, as well as repeated scans.

**NKI.** In support of open science, the 1000 Functional Connectomes Project was initiated on December 11, 2009 by various members of the MRI community seeking to form collaborative partnerships among imaging institutions for sharing well-documented multimodal image sets accompanied by phenotypic data. One such contribution is the Nathan Klein Institute (NKI)/Rockland sample, consisting of 186 T1-weighted images (87 females, 99 males).

**OASIS.** The initial Open Access Series of Imaging Studies (OASIS) data set consisted of 433 T1-weighted images. We processed all of these data, but 100 were excluded from our analysis due to probable Alzheimer's disease ( $CDR > 0$ ) and an additional 20 repeat scans were excluded, resulting in 313 individual subject scans included in the normal group statistical analysis (118 males, 195 females). Ages were between 18 and 96 and all subjects are right-handed.

**Fig. 3.** Representative sample of volume brain renderings from the four different cohorts (IXI = rows 1 and 2, MMRR = rows 3 and 4, NKI = rows 5 and 6, OASIS = rows 7 and 8), illustrating the qualitative difference between ANTs and FreeSurfer results, which are arranged top-and-bottom for each subject. Each brain was rigidly registered to the OASIS template for rendering purposes. With each subject we provide subject ID, age, and gender.

200 **MindBoggle-101 data for ROI definitions**

201 In Klein and Tourville (2012) the authors proposed the DKT cortical  
 202 labeling protocol—a modification of the popular Desikan–Killiany proto-  
 203 col (Desikan et al., 2006) to improve cortical labeling consistency and to  
 204 improve FreeSurfer's cortical classification of 31 cortical regions per  
 205 hemisphere, listed in Table 1. Forty manually labeled brains were used  
 206 to construct the DKT40 Gaussian classifier atlas, which is now bundled  
 207 with current versions of FreeSurfer and used to automate anatomical la-  
 208 beling of MRI data. Since the regional thickness values generated by  
 209 FreeSurfer follow this protocol, these anatomical labels provide a com-  
 210 mon standard for comparison between ANTs and FreeSurfer.

211 The work of Klein and Tourville (2012) also resulted in a publicly  
 212 available set of manually edited labels following the DKT protocol in  
 213 101 T1-weighted brain images from different sources, including a sub-  
 214 set of 20 images from the OASIS data set (specifically, the test–retest  
 215 data). These 20 images are used in the MALF step that defines the vol-  
 216 umetric cortical regions for each subject.

217 **ANTs volume-based cortical thickness estimation pipeline**

218 The ANTs cortical thickness estimation workflow is illustrated in  
 219 Fig. 1. The steps are as follows:

- 220 1. Initial N4 bias correction on input anatomical MRI
- 221 2. Brain extraction using a hybrid segmentation/template-based  
     strategy
- 222 3. Alternation between prior-based segmentation and “pure tissue”  
     posterior probability weighted bias correction using Atropos and N4
- 223 4. DiReCT-based cortical thickness estimation
- 224 5. Optional normalization to specified template and multi-atlas cortical  
     parcellation

225 Each component, including both software and data, is briefly de-  
 226 tailed below with the relevant references for additional information. Al-  
 227 though other preprocessing components are possible (e.g., noise  
 228 reduction as in Smith, 1996), the major steps constituting the ANTs  
 229 pipeline are limited to those enumerated above.

230 The coordination of all the algorithmic components is encapsulated  
 231 in the shell script `antsCorticalThickness.sh` with subcomponents  
 232 delegated to `antsBrainExtraction.sh` and `antsAtroposN4.sh`. A represen-  
 233 tative script command is reproduced in Listing 1 for a single IXI subject  
 234 to demonstrate the simplicity and mature status of what we propose in  
 235 this work and a comparison with the analogous FreeSurfer command.  
 236 Option descriptions are provided by invoking the help option, i.e.,  
 237 “`antsCorticalThickness.sh -h`”.

238 **Anatomical template construction**

239 Certain preprocessing steps, such as brain extraction and seg-  
 240 mentation, rely on templates and corresponding spatial priors. In ad-  
 241 dition, normalizing images to a standard coordinate system reduces  
 242 intersubject variability in population studies. Various approaches  
 243 exist for determining an optimal template, such as the selection  
 244 of a preexisting template based on a single individual (e.g., the  
 245 Talairach atlas; Talairach and Tournoux, 1988) or a publicly available  
 246 average of multiple individuals (e.g., the MNI template by Collins  
 247 et al., 1994 or the ICBM template by Mazziotta et al., 1995), or an av-  
 248 erage template constructed from the individuals under study. The  
 249 work of Avants et al. (2010b) explicitly models the geometric  
 250 component of the normalized space during optimization to produce  
 251 such mean templates. Coupling the intrinsic symmetry of SyN  
 252 pairwise registration (Avants et al., 2011a) and an optimized  
 253 shape-based sharpening/averaging of the template appearance,  
 254 Symmetric Group Normalization (SyGN) is a powerful framework  
 255 for producing optimal population-specific templates. The five tem-  
 256 plates used in this evaluation study are represented in Fig. 2.

257 **N4 bias field correction**

258 Critical to quantitative processing of MRI is the minimization of field  
 259 inhomogeneity effects which produce artificial low frequency intensity  
 260 variation across the image. Large-scale studies, such as ADNI, employ  
 261 perhaps the most widely used bias correction algorithm, N3 (Sled  
 262 et al., 1998), as part of their standard protocol (Boyes et al., 2008).

263 In Tustison et al. (2010) we introduced an improvement of N3, denot-  
 264 ed as “N4”, which demonstrates a significant increase in performance and  
 265 convergence behavior on a variety of data. This improvement is a result of  
 266 an enhanced fitting routine (which includes multi-resolution capabili-  
 267 ties) and a modified optimization formulation. For our workflow, the  
 268 additional possibility of specifying a weighted mask in N4 permits the  
 269 use of a “pure tissue” probability map (described below) calculated  
 270 during the segmentation pipeline for further improvement of bias field  
 271 estimation.

272 N4 is used in two places during the individual subject processing (cf  
 273 Fig. 1). It is used to generate an initial bias-corrected image for use in  
 274 brain extraction. The input mask is created by adaptively thresholding  
 275 the background from the foreground using the algorithm of Otsu  
 276 (1979). Following brain extraction, six-tissue (cerebrospinal fluid,  
 277 cortical gray matter, white matter, deep gray matter, brain stem, and  
 278 cerebellum) segmentation involves iterating between bias field correc-  
 279 tion using the current pure tissue probability map as a weight mask and  
 280 then using that bias-corrected image as input for the Atropos segmenta-  
 281 tion step (described below).

282 **Brain extraction**

283 Brain extraction using ANTs combines template building, high-  
 284 performance brain image registration, and Atropos segmentation with  
 285 topological refinements. An optimal template (Avants et al., 2010b),  
 286 i.e., a mean shape and intensity image representation of a particular co-  
 287 hort, is first constructed using structural MRI data. Template construc-  
 288 tion iterates between estimating the optimal template and registering  
 289 each subject to the optimal template. In this work, we perform the addi-  
 290 tional step of building separate templates for each cohort and propagat-  
 291 ing the probabilistic mask to each cohort template using registration of  
 292 the T1-weighted templates (cf Fig. 2). A probabilistic brain extraction  
 293 mask for the new template can then be generated by warping an  
 294 existing mask to the template or by averaging the warped, whole  
 295 brain labels of subjects registered to the new template, if such labels  
 296 are available. Further refinements include thresholding the warped  
 297 brain probability map at 0.5 and dilating the resulting mask with a  
 298 radius of two voxels. Atropos is used to generate an initial three-tissue  
 299 segmentation estimate within the mask region. Each of the three tissue  
 300 labels undergoes separate morphological operations including hole-  
 301 filling and erosion. These results are then combined to create the brain  
 302 extraction mask which is further refined by additional dilation, erosion,  
 303 and hole-filling operations.

304 In previous work (Avants et al., 2010a) we compared an earlier ver-  
 305 sion of our extraction method with publicly available brain extraction  
 306 algorithms, including AFNI's 3dIntracranial (Ward, 1999), FSL's BET2  
 307 (Smith, 2002), FreeSurfer's mri\_watershed (Ségonne et al., 2004), and  
 308 BrainSuite (Dogdas et al., 2005). Our hybrid registration/segmentation  
 309 approach performed with an accuracy comparable to FreeSurfer and a  
 310 parameter-tuned version of BrainSuite. Fig. 3 presents a visual compar-  
 311 ison of results derived with the current ANTs brain extraction method  
 312 and results obtained using FreeSurfer.

313 **Atropos six-tissue segmentation**

314 In Avants et al. (2011b) we presented an open source *n*-tissue  
 315 segmentation software tool (which we denote as “Atropos”) that at-  
 316 tempts to distill over 20 years of active research in this area, in particu-  
 317 lar some of the most seminal work (e.g., Ashburner and Friston, 2005;  
 318 Zhang et al., 2001). Specification of prior probabilities includes spatially  
 319 varying Markov Random Field modeling, prior label maps, and prior  
 320 probability maps typically derived from our template building process.

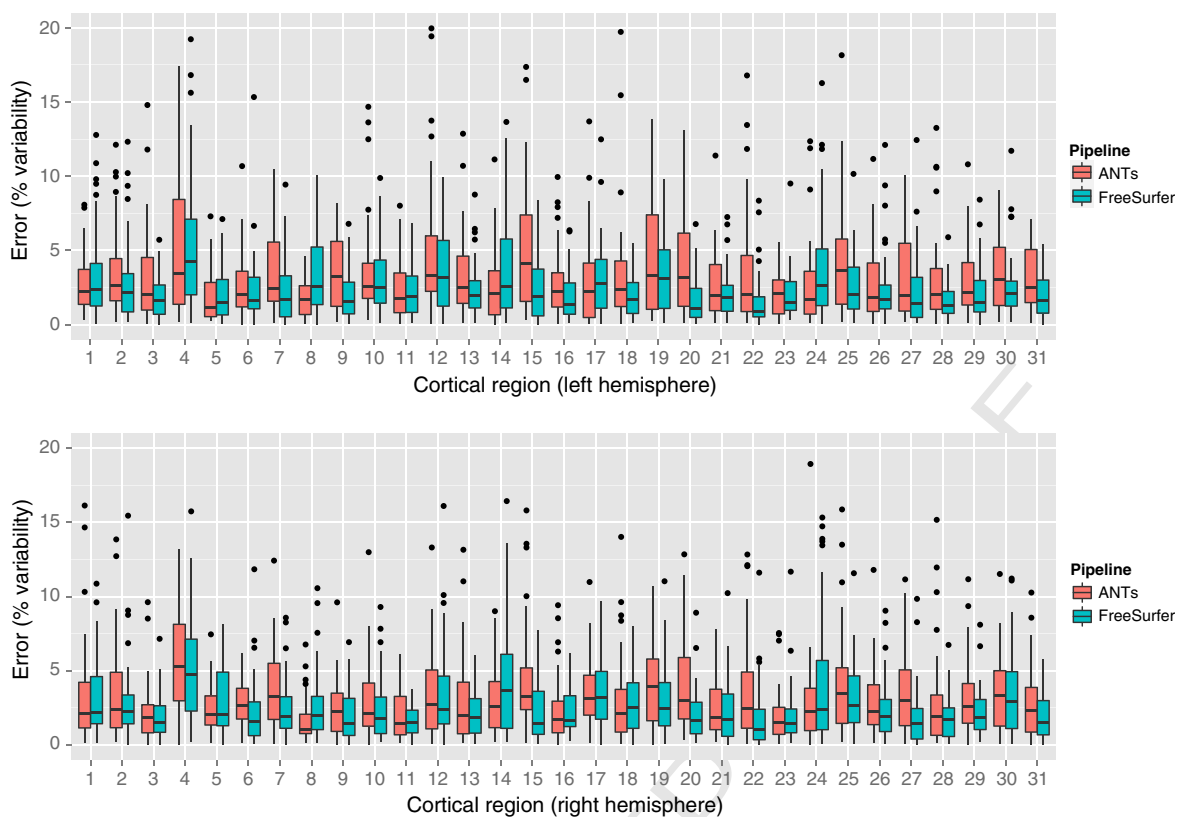


**Fig. 5.** Percent error variability for both ANTs and FreeSurfer pipelines over the left and right hemispheres of both the MMRR and OASIS data subsets within the 62 regions defined by the Desikan–Killiany–Tourville atlas. Both methods demonstrate good repeatability qualities.

Additional capabilities include handling of multivariate data, partial volume modeling (Shattuck et al., 2001), a memory-minimization mode, label propagation, a plug-and-play architecture for incorporation of novel likelihood models which include both parametric and non-parametric models for both scalar and tensorial images, and alternative posterior formulations for different segmentation tasks.

Due to the important interplay between segmentation and bias correction, we perform multiple N4 = Atropos iterations. A pure tissue probability weight mask generated from the posterior probabilities is derived from the segmentation step. Given  $N$  labels and the corresponding  $N$  posterior probability maps  $\{P_1, \dots, P_N\}$  produced during segmentation, the N4 weight mask is created at each N4 = Atropos iteration from

$$P_{\text{pure tissue}}(\mathbf{x}) = \sum_{i=1}^N P_i(\mathbf{x}) \prod_{j=1, j \neq i}^N (1 - P_j(\mathbf{x})). \quad (1)$$

One of the key insights of the original N3 development is the observation that inhomogeneities cause the intensity values of pure tissue peaks to spread in the intensity histogram as though convolved with a Gaussian. A core contribution of N3 is the proposed corrective step of deconvolving the intensity histogram to accentuate the tissue peaks, coupled with a spatial smoothing constraint. The pure tissue probability mask is used in N4 to weight more heavily the influence of voxels corresponding to pure tissue types (as determined by the segmentation) during the deconvolution process while minimizing the contribution of regions such as the gray/white matter interface where peak membership is ambiguous.

Atropos enables prior knowledge to guide the segmentation process where template-based priors are integrated into the optimization with a user-controlled weight. Modulating the likelihood and prior contributions to the posterior probability is essential for producing adequate segmentations. Atropos weights the likelihood and priors according to  $P(x|y) \propto P(y|x)^1 - \alpha P(x)^\alpha$  where  $\alpha$  is a user-selected parameter

which weights the tradeoff between the likelihood and priors terms. A weighting of  $\alpha = 0.25$  is the default value based on our extensive experimentation with different parameter weights.

Since cortical thickness estimation only requires the cortical gray and white matter, the deep gray and white matter (both labels and posterior maps) are combined to form a single “white matter” set. This white matter set and the cortical gray matter are the only results from the segmentation step that are used by the DiReCT algorithm (described below).

To generate the priors for each T1 template, we used the multi-atlas label fusion (MALF) algorithm of Wang et al. (2013) in conjunction with a labeled subset of the OASIS data set.<sup>1</sup> First, we normalized the labeled OASIS subset to the template. We then performed MALF on the template using the normalized labeled data as input. This resulted in a labeled, parcellated template consisting of 100+ labels defining the different brain regions. We then condensed this template-specific labeling to the six needed for our analysis, viz., cerebrospinal fluid (CSF), gray matter (GM), white matter (WM), deep gray matter, brain stem, and cerebellum. For example, all cortical regions were assigned a single label representing the gray matter.

These binary masks were then smoothed using Gaussian convolution with a one voxel-width kernel. Since the labelings did not describe the extracerebral CSF, we augmented the CSF prior image with the CSF posterior output from running each template through the segmentation component of the above-described pipeline. This new CSF prior was then subtracted from each of the other five prior probability images and limited to the probability range of [0,1]. The prior probabilities for the five templates used in this evaluation are given in Fig. 4.

<sup>1</sup> These data were originally acquired by the first and last authors to aid in the MICCAI 2012 Grand Challenge and Workshop on Multi-Atlas Labeling. The data was released under the Creative Commons Attribution-NonCommercial license. Labelings were provided by Neuromorphometrics, Inc. (<http://Neuromorphometrics.com/>) under academic subscription.

t2.1  
t2.2  
Mean repeatability error over all regions.

|            | MMRR | OASIS |
|------------|------|-------|
| ANTs       | 3.2% | 3.3%  |
| FreeSurfer | 2.5% | 2.8%  |

### 382 DiReCT cortical thickness estimation

383 DiReCT was introduced in Das et al. (2009) and was made available  
 384 in ANTs as the program KellySlater. Since then several improvements  
 385 have been made and incorporated into the program KellyKapowski.<sup>2</sup>  
 386 The more recent implementation has made numerous advances includ-  
 387 ing multi-threading, written in rigorous ITK coding style, and has been  
 388 made publicly available through ANTs, complete with a unique com-  
 389 mand line interface design developed specifically for ANTs tools.

### 390 Processing miscellany

391 Given the documented variability in FreeSurfer results with version  
 392 and operating system (Gronenchild et al., 2012) (as we would expect  
 393 with our own ANTs pipeline), all data were processed using the same  
 394 ANTs and FreeSurfer versions on the same hardware platform. Processing  
 395 was performed using the Linux (CentOS release 6.4) cluster at the Univer-  
 396 sity of Virginia (<http://www.uvacse.virginia.edu>) using single-threading  
 397 with a maximal requested memory footprint of 8 Gb for ANTs and 4 Gb  
 398 for FreeSurfer. The development version of ANTs was used for processing  
 399 (git commit tag: 69d3a5a6c7125ccf07a9e9cf6ef29f0b91e9514f, date Dec.  
 400 11, 2013). FreeSurfer version 5.3 x86\_64 for CentOs was downloaded on 5  
 401 December, 2013 ("freesurfer-Linux-centos6\_x86\_64-stable-pub-v5.3.0",  
 402 release date: 15 May, 2013). The brain extraction and segmentation  
 403 results from both pipelines were visually inspected to screen for major  
 404 problems. No manual changes were made for any component of either  
 405 pipeline and no change was made to the settings of either processing  
 406 pipeline.

### 407 Evaluation

408 Traditional assessment approaches, such as manual labeling, are  
 409 inadequate for evaluating large-scale performance. We therefore sought  
 410 to minimize failure rate, quantify the repeatability of cortical thickness  
 411 measures, and determine whether the ANTs pipeline reveals biological-  
 412 plausibly plausible relationships between the cortex, gender,<sup>3</sup> and age and  
 413 how its performance compares to the current de facto standard of  
 414 FreeSurfer-derived thickness estimation. Collectively, these surrogate  
 415 measurements allow us to establish data-derived relative performance  
 416 standards. Additionally, for completeness, we include timing results as  
 417 that factors into usability.

### 418 Repeatability

419 Repeat scans of 40 subjects (20 MMRR subjects and 20 OASIS sub-  
 420 jects) were used to determine the repeatability of regional cortical  
 421 thickness measurements,  $T$ . Similar to the reproducibility assessment

given in Jovicich et al. (2013), we demonstrate this in terms of the per- 422 cent variability error:  
 423

$$\varepsilon = \frac{|T_{\text{scan}} - T_{\text{rescan}}|}{0.5 \times (T_{\text{scan}} + T_{\text{rescan}})}. \quad (2)$$

425 Comparison of the ANTs and FreeSurfer percent variability errors for  
 426 the 62 DKT regions for both the OASIS and MMRR scan–rescan data sets 427 is given in Fig. 5. Mean values are given in Table 2. Although the variance 428 is slightly greater for the set of ANTs measurements, statistical testing 429 per cortical region (two-tailed paired  $t$ -test, corrected using false dis- 429 covery rate) did not indicate non-zero mean differences for either ap- 430 proach for any region. 431

We also calculated the intraclass correlation coefficient ("ICC(2,1)" 432 in the notation of Shrout and Fleiss, 1979) to assess scan/rescan reliabil- 433 ity. The ANTs thickness pipeline produced an ICC value of 0.98 and the 434 FreeSurfer thickness pipeline yielded an ICC value of 0.97, indicating 435 good scan/rescan reliability for both ANTs and FreeSurfer. 436

### Age prediction assessment

Despite good repeatability with both ANTs and FreeSurfer, such 438 measures do not provide an assessment of accuracy or even relative util- 439 ity. For example, strong priors can yield good repeatability measures but 440 potentially at the expense of data fidelity thus compromising the quality 441 of models (statistical or otherwise) built from such results. Given that 442 ground truth is not available for these data or for the many studies 443 looking at brain morphology, an indirect method (or set of methods) 444 is required for determining the quality of thickness estimation. 445

For our first assessment, we modeled age versus regional cortical 446 thickness values to determine which framework produces better pre- 447 dictive thickness estimates. We first subdivided the thickness data 448 into training and testing subsets with an even split between the two 449 subsets.<sup>4</sup> We then used the training data to create two models for 450 each pipeline: 1) standard linear regression and 2) random forests (a 451 non-parametric machine learning technique) (Breiman, 2001), for esti- 452 mating age from both ANTs and FreeSurfer thickness values in the test- 453 ing data. 454

The formula (in the notation of Wilkinson and Rogers, 1973) for the 455 linear model is 456

$$\text{AGE} \sim \text{VOLUME} + \text{GENDER} + \sum_{i=1}^{62} T(\text{DKT}_i) \quad (3)$$

where  $T(\text{DKT}_i)$  is the average thickness value in region  $\text{DKT}_i$  and  $\text{VOL-}$  458  $\text{UME}$  is total intracranial volume. Similarly, the random forest model 459 was specified as a combination of all terms using the randomForest 460 package in R with the default settings and 200 trees. 460

In order to ensure a fair comparison, the procedure described above 461 consisting of training and testing steps was performed for  $n = 1000$  per- 462 mutations to elicit a performance distribution which we measure using 463 the relative mean square error (RMSE): 464

$$\text{RMSE} = \sqrt{\frac{\sum (\text{AGE}_{\text{true}} - \text{AGE}_{\text{predicted}})^2}{N}}. \quad (4)$$

Due to the limited range in ages across data sets, we restricted train- 467 ing and testing to the age range [20,80]. The resulting distributions are 467 illustrated in Fig. 6. In addition to a combined assessment, we also 468

<sup>2</sup> Traditional academic discourse encountered in the published literature rarely contextualizes peculiarities such as algorithmic nomenclature. We briefly mention that this was the source of a rare disagreement between the first and last authors based, as many disagreements are, on a simple misunderstanding and not an affronting existential statement concerning a certain favorite sitcom of the first author's youth.

<sup>3</sup> We recognize the distinction often made between "sex" and "gender" (cf <http://www.who.int/gender/whatisgender/en/>). As the demographic information collected during the course of the imaging studies is presumably self-reported, we assume that most self-identify in terms of gender and, therefore, use the term "gender" in data descriptions.

<sup>4</sup> We tried various training proportions between 10 and 90% (in increments of 10%) to see if that had an effect on relative performance for both age and gender prediction comparisons. Although age predictive capabilities for both pipelines showed improvement (gender prediction was mostly unaffected), the relative outcomes were the same.

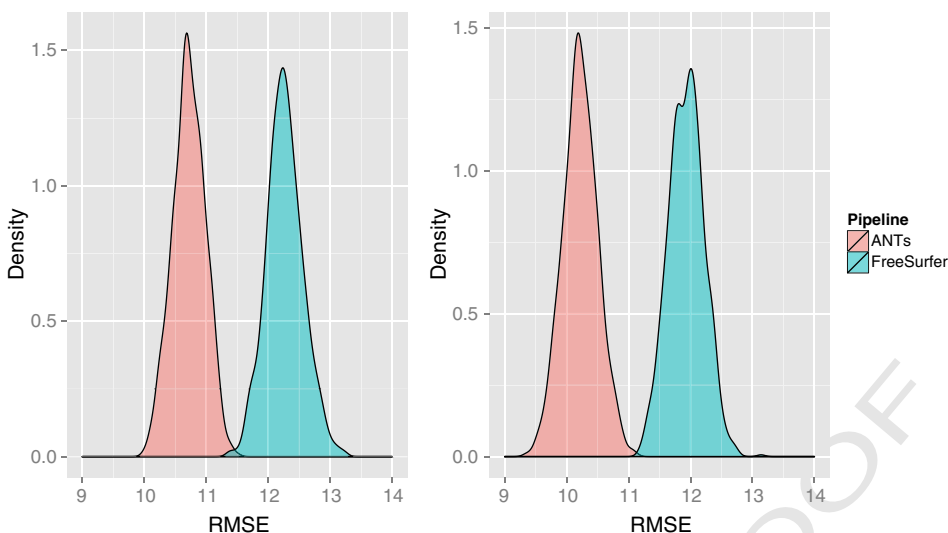


**Fig. 6.** Age prediction RMSE distributions of linear (left) and random forest (right) models for the ANTs- and FreeSurfer-derived thickness values over the combined four cohorts. For both prediction models ANTs RMSE error is lower.

469 perform separate model prediction for each of the three larger data sets  
470 (i.e., IXI, NKI, and OASIS).

471 ANTs-based RMSE values were lower for both models and each of  
472 the four different subset comparisons except for the random forest  
473 model constructed from the OASIS data set. All mean RMSE values are  
474 provided in Table 3.

475 To further elucidate the regional differences in predictive power spe-  
476 cifically in the random forest model, we provide variable importance  
477 plots for both pipelines using the mean decrease in accuracy measure  
478 in Fig. 7. During random forest model construction (specifically the  
479 out-of-bag error calculation stage), the decrease in prediction accuracy  
480 with the omission of a single feature or variable is tracked and averaged.  
481 Thus, those features which have the greatest decrease in mean accuracy  
482 are considered to be the most discriminative. It should be noted that  
483 correlative effects are not considered in the rankings.

#### 484 Gender prediction assessment

485 We also performed a similar prediction assessment using gender as  
486 the regressand. The binomial generalized linear model is

$$GENDER \sim VOLUME + AGE + \sum_{i=1}^{62} T(DKT_i) \quad (5)$$

488 where  $T(DKT_i)$  is the average thickness value in region  $DKT_i$  and  
489  $VOLUME$  is the total intracranial volume. We then characterized  
490 performance using a ROC curve for both methods (see Fig. 9)  
491 where we averaged over 1000 permutations. The mean area  
492 under the curve (AUC) for both methods was also quantified with  
493 values of  $ANTs_{AUC} = 0.87$  and  $FreeSurfer_{AUC} = 0.83$ . (See Fig. 8.)

t3.1 **Table 3**  
t3.2 Mean RMSE for age prediction in years.

|                       | Linear model    | Random forest |
|-----------------------|-----------------|---------------|
| ANTs (combined)       | 10.7            | 10.2          |
| FreeSurfer (combined) | 12.3            | 11.9          |
| ANTs (IXI)            | 9.3             | 8.6           |
| FreeSurfer (IXI)      | 12.3            | 11.7          |
| ANTs (NKI)            | NA <sup>a</sup> | 10.9          |
| FreeSurfer (NKI)      | NA <sup>a</sup> | 13.3          |
| ANTs (OASIS)          | 15.0            | 12.4          |
| FreeSurfer (OASIS)    | 15.0            | 11.4          |

#### Computation time

All images underwent the ANTs and FreeSurfer pipeline processing using the computational cluster at the University of Virginia. Processing times varied approximately between 10 and 20 h per subject for both pipelines for the entire cortical thickness estimation procedure although ANTs processing, on average, took slightly longer. Averaged over all cohorts, ANTs required  $15.7 \pm 2.0$  h per subject and FreeSurfer required  $14.1 \pm 2.9$  h per subject.

The propagation of the DKT labels to each subject using label fusion as described earlier was performed in parallel and took anywhere between 40 and 80 h per subject for 16 serial image registrations and the application of the joint label fusion algorithm (Wang et al., 2013). For each subject, 20 atlas registrations are used to generate the labeling for that subject. Therefore to do the MALF labeling for the entire cohort, approximately  $1200 \times 20 = 24,000$  registrations were performed. The antsMalfLabeling.sh script mentioned earlier parallelizes the registration component which decreases the time for parallel computation platforms.

#### Discussion

In the absence of ground truth, we used repeatability and prediction of demographic variables to compare the ANTs and FreeSurfer cortical thickness pipelines. The only major failure was the FreeSurfer brain extraction of a single IXI subject (IXI430-IOP-0990). Also, three NKI subjects were not processed to completion with FreeSurfer (1713515, 18755434, and 2674565) and were not included in the analysis. Although researchers might quibble over processing minutiae such as the inclusion of too much (or not enough) of the meninges, we approached our evaluation using more objective criteria which concern all those engaged in this type of research. We are currently trying to develop methods to facilitate data inspection for quick quality assurance/control.

#### Repeatability of thickness measurements

The OASIS data set and the MMRR data set allow us to test whether the same thickness values emerge from T1-weighted MRI collected on the same subject but at different times of the day or over a time separation within a few weeks. Although the ANTs cortical thickness pipeline produced similar repeatability assessments as FreeSurfer in these data, there are many additional issues to explore with the ANTs-based



**Fig. 7.** Regional importance random forest plots for (left) ANTs and (right) FreeSurfer using “MeanDecreaseAccuracy” ranking all model variables specified by Eq. (3).

framework. Pre-analysis confounds such as short-term alterations in cortical morphology due to the T1-weighted susceptibility to blood flow (Franklin et al., 2013; Salgado-Pineda et al., 2006; Yamasue et al., 2007) and MRI acquisition parameters such as field strength, site, resolution, scanner, longitudinal variation in scanner conditions, and pulse sequence (Han et al., 2006; Jovicich et al., 2013; Lüsebrink et al., 2013) have been evaluated with FreeSurfer which has shown good reliability under various permutations of these conditions. Although we did not explicitly investigate the repeatability performance of the ANTs framework under such effects, the relatively good performance on the large and varied data (in terms of site, field strength, scanner, and acquisition sequence) used in this study provides confidence in its robustness to a variety of imaging conditions.

ANTs and FreeSurfer cortical thickness mean reliability measurements are correlated across all regions (Pearson correlation = 0.44). Although our thickness reliability measurements represent the compound effect of registration, segmentation, anatomical labeling, and

the thickness computation algorithm, this correlation suggests that 548 these effects are non-random. That is, reliability measurements are in- 549 fluenced by characteristics intrinsic to the underlying neuroanatomy 550 as represented in approximately one millimeter resolution volumetric 551 T1-weighted MRI. Perhaps the least reliable region is the entorhinal cor- 552 tex (region 4 in Fig. 5) which has a relatively small volume, is challeng- 553 ing to distinguish from surrounding structures (Price et al., 2010), and is 554 also relatively thin. Spatial variation in segmentation accuracy is known 555 to relate to a structure's volume and tissue characteristics and this has 556 led to a body of research on both segmentation and acquisition proto- 557 cols that are optimized for specific regions. Perhaps the most substantial 558 work in MRI has focused on temporal lobe structures including the hip- 559 pocampus. Both FreeSurfer and our own group have optimized proto- 560 cols to address such concerns ([http://www.hippocampalsubfields.](http://www.hippocampalsubfields.com/) 561 [com/](http://www.hippocampalsubfields.com/)). Given caveats associated with cost vs. benefit, our current results 562 suggest that optimized protocols may be relevant for additional cortical 563 regions. 564

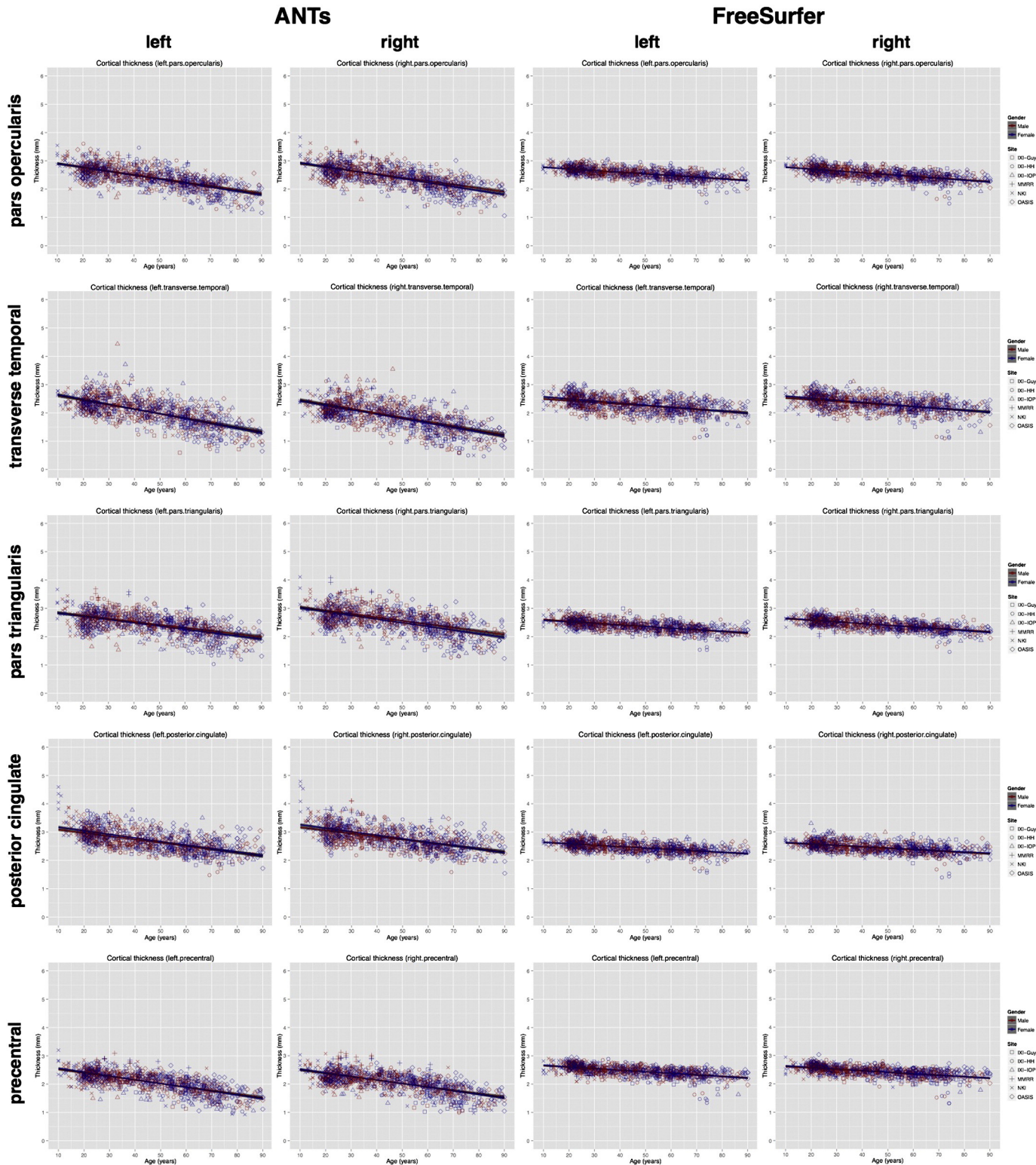


**Fig. 8.** Age vs. thickness plots for cortical regions that are most relevant in age prediction. These are the most discriminative regions across both methods as determined by random forest importance measurements (of Fig. 7). Note that all regional plots for both ANTs and FreeSurfer are available online (see Appendix A).

565 Voxel/vertex-based analysis

566 One of the limitations of our evaluation was the limitation of com-  
 567 parative analysis to mean ROI thickness values defined by the 62 cortical  
 568 regions of the DKT atlas. Quite common in the literature, however, are  
 569 point-wise (vertex- or voxel-based) analyses (e.g., Chung et al., 2005).

The ANTs pipeline described in this work is equally applicable to such 570 studies. The only additional requirement is the specification of the nor-  
 571 malization template. For this work we opted for the ROI analysis to 572 avoid potential bias issues when navigating between surface and 573 volume representations (Klein et al., 2010). Future work will certainly 574 explore such analyses. 575

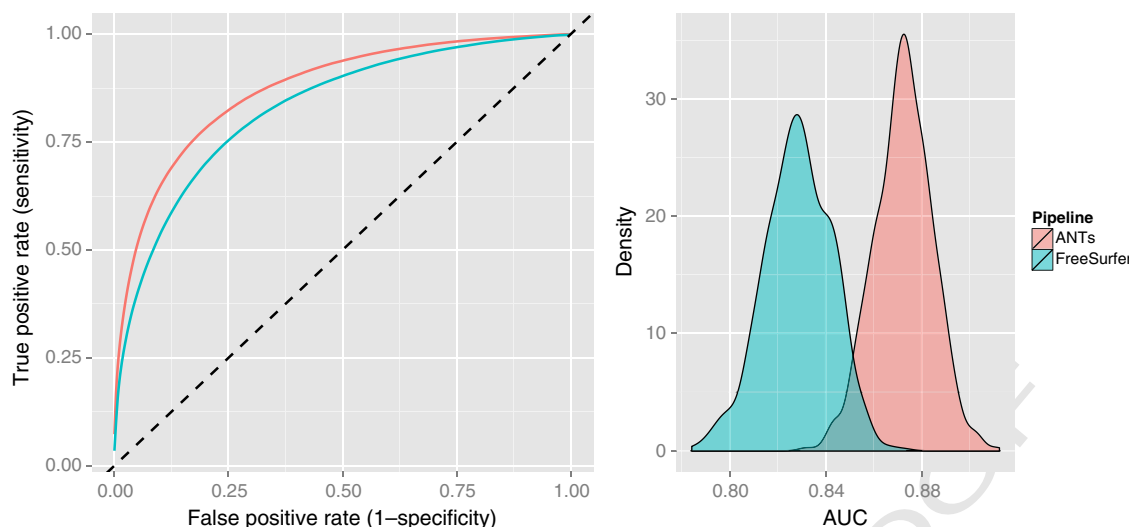


**Fig. 9.** Average ROC curve and corresponding AUC distributions for gender prediction using ANTs and FreeSurfer thickness values. Values were averaged for 1000 permutations resulting in mean values of  $\text{ANTs}_{\text{AUC}} = 0.87$  and  $\text{FreeSurfer}_{\text{AUC}} = 0.83$  ( $p < 10^{-16}$ ).

## 576 Age and gender prediction

577 Although repeatability between ANTs and FreeSurfer is comparable,  
578 such measures are not as useful in determining the utility of the mea-  
579 suring software. That is the reason we used a training and testing para-  
580 digm to evaluate how well both frameworks produce measurements  
581 capable of predicting demographics which are well-known to correlate  
582 with cortical thickness. Additionally, these demographic measures are  
583 probably some of the easiest and most reliably obtained of all possible  
584 demographic measures used for this type of assessment.

585 Previous research has used predictive modeling for comparing corti-  
586 cal thickness algorithms. For example, in Clarkson et al. (2011), classifi-  
587 cation of healthy, semantic dementia, and progressive non-fluent  
588 aphasia categories using regional cortical thickness values was used to  
589 determine the predictive modeling capabilities of different cortical  
590 thickness processing protocols in 101 subjects. However, differential di-  
591 agnosis of dementia (Neary et al., 2005) is not as straightforward as  
592 obtaining a subject's age or gender and regressing that against cortical  
593 thickness; the latter constitutes biological relationships that have been  
594 well-studied and reported in the literature.

595 For age prediction, we used both a linear model (due to its general  
596 ubiquity) and a random forest model (a non-parametric model to con-  
597 trast with the linear approach) which showed overall good perfor-  
598 mance. Also, the linear and random forest models have the advantage  
599 of being interpretable—that is, the models reveal the specific predictors  
600 that are most valuable which makes comparison with previous age  
601 versus thickness assessments possible.

602 For example, in Hogstrom et al. (2013), 322 T1-weighted MRI of  
603 healthy adults with an age range of [20,85] were used, in part, to char-  
604 acterize the relationship between age and cortical thickness using  
605 FreeSurfer and a similar linear modeling approach. Significant findings  
606 for age were reported in the “precentral gyrus, medial parts of the su-  
607 perior frontal gyrus, DMPFC, and rostral middle frontal cortex.” Based on  
608 the cortical parcellation provided by the DKT atlas, we also saw similar  
609 strong effects in the precentral gyrus (cf Fig. 7).

610 This study was limited to a cross-sectional investigation thus  
611 limiting extrapolations of ANTs performance to longitudinal data unlike  
612 recent FreeSurfer extensions which accommodate longitudinal data  
613 (Jovicich et al., 2013; Reuter et al., 2012). Also, some users may choose  
614 to segment and register with ANTs and subsequently employ any  
615 alternative (e.g., surface-based) method for thickness estimation. Fur-  
616 ther work is needed by independent authors working on established  
617 pipelines to better compare surface-based and volume-based thickness

618 reliability and accuracy across different populations, age ranges, and  
619 with longitudinal protocols.

## Computation time

620 Computation time for the registration and segmentation compo-  
621 nents of the ANTs pipeline are substantial but are not significantly  
622 worse than those of FreeSurfer. It is likely that nearly as reliable results  
623 can be obtained in much less time for many of the subjects in this study.  
624 However, our interest in maximizing reliability and quality led us to  
625 employ parameters in the registration, segmentation, and bias correc-  
626 tion that are as robust as possible to differences in head position, the  
627 presence of large deformations between template and target brains  
628 and substantial inhomogeneity or other artifacts in the image content  
629 itself.

**Table 4**  
Resources used in this work.

|  |   |       |
|--|---|-------|
| Packages                                     |   | t4.1  |
| ANTs   | <a href="http://stnava.github.io/ANTs">http://stnava.github.io/ANTs</a>   | t4.4  |
| FreeSurfer                                   | <a href="http://surfer.nmr.mgh.harvard.edu">http://surfer.nmr.mgh.harvard.edu</a>   | t4.5  |
| Available scripts and examples               |   | t4.6  |
| antsBrainExtraction.sh                       | <a href="https://github.com/ntustison/antsBrainExtractionExample">https://github.com/ntustison/antsBrainExtractionExample</a>               | t4.7  |
| antsAtroposN4.sh                             | <a href="https://github.com/ntustison/antsAtroposN4Example">https://github.com/ntustison/antsAtroposN4Example</a>                           | t4.8  |
| antsCorticalThickness.sh                     | <a href="https://github.com/ntustison/antsCorticalThicknessExample">https://github.com/ntustison/antsCorticalThicknessExample</a>           | t4.9  |
| antsMultivariateTemplateConstruction.sh      | <a href="https://github.com/ntustison/TemplateBuildingExample">https://github.com/ntustison/TemplateBuildingExample</a>                     | t4.10 |
| antsMafLabeling.sh                           | <a href="https://github.com/ntustison/MafLabelingExample">https://github.com/ntustison/MafLabelingExample</a>                               | t4.11 |
| Analysis scripts                             | <a href="https://github.com/ntustison/KapowskiChronicles">https://github.com/ntustison/KapowskiChronicles</a>                               | t4.12 |
| Public data                                  |   | t4.13 |
| MindBoggle101                                | <a href="http://mindboggle.info/data.html">http://mindboggle.info/data.html</a>   | t4.14 |
| Cohort templates and priors                  | <a href="http://figshare.com/articles/ANTs_ANTsR_Brain_Templates/915436">http://figshare.com/articles/ANTs_ANTsR_Brain_Templates/915436</a> | t4.15 |
| IXI  | <a href="http://biomedic.doc.ic.ac.uk/brain-development">http://biomedic.doc.ic.ac.uk/brain-development</a>                                 | t4.16 |
| MMRR   | <a href="http://www.nitrc.org/projects/multimodal">http://www.nitrc.org/projects/multimodal</a>   | t4.17 |
| NKI  | <a href="http://fcon_1000.projects.nitrc.org">http://fcon_1000.projects.nitrc.org</a>   | t4.18 |
| OASIS  | <a href="http://www.oasis-brains.org">http://www.oasis-brains.org</a>   | t4.19 |
| MICCAI 2012 Workshop on Multi-Atlas Labeling | <a href="https://masi.vuse.vanderbilt.edu/workshop2012/index.php">https://masi.vuse.vanderbilt.edu/workshop2012/index.php</a>               | t4.20 |

631 **Conclusions**

632 Imaging biomarkers such as cortical thickness play an important  
 633 role in neuroscience research. Extremely useful to researchers are  
 634 robust software tools for generating such biomarkers. In this work  
 635 we detailed our open source offering for estimating cortical thick-  
 636 ness directly from T1 images and demonstrated its utility on a large  
 637 collection of public brain data from multiple databases acquired at  
 638 multiple sites. To our knowledge, this study constitutes the largest  
 639 collection of cortical thickness data processed in a single study. We  
 640 anticipate that public availability of our tools and extensive tuning  
 641 on the specified cohorts will prove useful to the larger research  
 642 community. In this work, we only explored a portion of the potentially  
 643 interesting investigations possible with these data. Since all of the data are publicly available, further work can be easily pursued  
 644 by us or by other interested groups.

646 **Appendix A**

647 Available resources are listed in **Table 4** with their corresponding  
 648 addresses. Examples and data for all scripts described in the manuscript  
 649 are also available for download. This should enable interested re-  
 650 searchers to duplicate the results in this work.

651 **References**

- 652 Ashburner, J., Friston, K.J., 2005. Unified segmentation. *Neuroimage* 26 (3), 839–851.  
 653 <http://dx.doi.org/10.1016/j.neuroimage.2005.02.018> (Jul).
- 654 Avants, B.B., Klein, A., Tustison, N.J., Woo, J., Gee, J.C., 2010a. Evaluation of an open-access,  
 655 automated brain extraction method on multi-site multi-disorder data. *Hum. Brain Mapp.*  
**Q12**
- 656 Avants, B.B., Yushkevich, P., Pluta, J., Minkoff, D., Korczykowski, M., Detre, J., Gee, J.C.,  
 657 2010b. The optimal template effect in hippocampus studies of diseased populations.  
 658 *Neuroimage* 49 (3), 2457–2466. <http://dx.doi.org/10.1016/j.neuroimage.2009.09.062>  
 659 (Feb).
- 660 Avants, B.B., Tustison, N.J., Song, G., Cook, P.A., Klein, A., Gee, J.C., 2011a. A reproducible  
 661 evaluation of ANTs similarity metric performance in brain image registration.  
 662 *Neuroimage* 54 (3), 2033–2044. <http://dx.doi.org/10.1016/j.neuroimage.2010.09.025>  
 663 (Feb).
- 664 Avants, B.B., Tustison, N.J., Wu, J., Cook, P.A., Gee, J.C., 2011b. An open source multivariate  
 665 framework for *n*-tissue segmentation with evaluation on public data. *Neuroinformatics*  
 666 9 (4), 381–400. <http://dx.doi.org/10.1007/s12021-011-9109-y> (Dec).
- 667 Bouix, S., Martin-Fernandez, M., Ungar, L., Nakamura, M., Koo, M.S., McCarley, R.W., Shenton,  
 668 M.E., 2007. On evaluating brain tissue classifiers without a ground truth. *Neuroimage* 36  
 669 (4), 1207–1224. <http://dx.doi.org/10.1016/j.neuroimage.2007.04.031> (Jul).
- 670 Boyes, R.G., Gunter, J.L., Frost, C., Janke, A.L., Yeatman, T., Hill, D.L.G., Bernstein, M.A.,  
 671 Thompson, P.M., Weiner, M.W., Schuff, N., Alexander, G.E., Killiany, R.J., DeCarli, C.,  
 672 Jack, C.R., Fox, N.C., ADNI Study, 2008. Intensity non-uniformity correction using N3  
 673 on 3-T scanners with multichannel phased array coils. *Neuroimage* 39 (4),  
 674 1752–1762. <http://dx.doi.org/10.1016/j.neuroimage.2007.10.026> (Feb).
- 675 Breiman, L., 2001. Random forests. *Machine Learning*, pp. 5–32.
- 676 Chung, M.K., Robbins, S.M., Dalton, K.M., Davidson, R.J., Alexander, A.L., Evans, A.C., 2005.  
 677 Cortical thickness analysis in autism with heat kernel smoothing. *Neuroimage* 25 (4),  
 678 1256–1265. <http://dx.doi.org/10.1016/j.neuroimage.2004.12.052> (May).
- 679 Clarkson, M.J., Cardoso, M.J., Ridgway, G.R., Modat, M., Leung, K.K., Rohrer, J.D., Fox, N.C.,  
 680 Ourselin, S., 2011. A comparison of voxel and surface based cortical thickness estimation  
 681 methods. *Neuroimage* 57 (3), 856–865. <http://dx.doi.org/10.1016/j.neuroimage.2011.05.053> (Aug).
- 682 Collins, D.L., Neelin, P., Peters, T.M., Evans, A.C., 1994. Automatic 3D intersubject registration  
 683 of MR volumetric data in standardized Talairach space. *J. Comput. Assist. Tomogr.*  
 684 18 (2), 192–205.
- 685 Dale, A.M., Fischl, B., Sereno, M.I., 1999. Cortical surface-based analysis. I. Segmentation  
 686 and surface reconstruction. *Neuroimage* 9 (2), 179–194. <http://dx.doi.org/10.1006/nimg.1998.0395> (Feb).
- 687 Das, S.R., Avants, B.B., Grossman, M., Gee, J.C., 2009. Registration based cortical thickness  
 688 measurement. *Neuroimage* 45 (3), 867–879. <http://dx.doi.org/10.1016/j.neuroimage.2008.12.016> (Apr).
- 689 Davatzikos, C., Bryan, N., 1996. Using a deformable surface model to obtain a shape rep-  
 690 resentation of the cortex. *IEEE Trans. Med. Imaging* 15 (6), 785–795. <http://dx.doi.org/10.1109/42.544496>.
- 691 Desikan, R.S., Ségonne, F., Fischl, B., Quinn, B.T., Dickerson, B.C., Blacker, D., Buckner, R.L.,  
 692 Dale, A.M., Maguire, R.P., Hyman, B.T., Albert, M.S., Killiany, R.J., 2006. An automated  
 693 labeling system for subdividing the human cerebral cortex on MRI scans into gyral  
 694 based regions of interest. *Neuroimage* 31 (3), 968–980. <http://dx.doi.org/10.1016/j.neuroimage.2006.01.021> (Jul).
- 695 Dickerson, B.C., Bakkour, A., Salat, D.H., Feczkó, E., Pacheco, J., Greve, D.N., Grodstein, F.,  
 696 Wright, C.I., Blacker, D., Rosas, H.D., Sperling, R.A., Atri, A., Growdon, J.H., Hyman, B.  
 697 T., Morris, J.C., Fischl, B., Buckner, R.L., 2009. The cortical signature of Alzheimer's  
 698 disease: regionally specific cortical thinning relates to symptom severity in very  
 699 mild to mild AD dementia and is detectable in asymptomatic amyloid-positive indi-  
 700 viduals. *Cereb. Cortex* 19 (3), 497–510. <http://dx.doi.org/10.1093/cercor/bhn113>  
 701 (Mar).
- 702 Dogdas, B., Shattuck, D.W., Leahy, R.M., 2005. Segmentation of skull and scalp in 3-D  
 703 human MRI using mathematical morphology. *Hum. Brain Mapp.* 26 (4), 273–285.  
<http://dx.doi.org/10.1002/hbm.20159> (Dec).
- 704 Du, A.T., Schuff, N., Kramer, J.H., Rosen, H.J., Gorno-Tempini, M.L., Rankin, K., Miller, B.L.,  
 705 Weiner, M.W., 2007. Different regional patterns of cortical thinning in Alzheimer's  
 706 disease and frontotemporal dementia. *Brain* 130 (Pt 4), 1159–1166. <http://dx.doi.org/10.1093/brain/awm016> (Apr).
- 707 Fischl, B., Dale, A.M., 2000. Measuring the thickness of the human cerebral cortex from  
 708 magnetic resonance images. *Proc. Natl. Acad. Sci. U. S. A.* 97 (20), 11050–11055.  
<http://dx.doi.org/10.1073/pnas.200033797> (Sep).
- 709 Fischl, B., Sereno, M.I., Dale, A.M., 1999. Cortical surface-based analysis. II: Inflation,  
 710 flattening, and a surface-based coordinate system. *Neuroimage* 9 (1), 195–207.  
<http://dx.doi.org/10.1006/nimg.1998.0396> (Jan).
- 711 Fischl, B., Salat, D.H., Busa, E., Albert, M., Dieterich, M., Haselgrave, C., van der Kouwe, A.,  
 712 Killiany, R., Kennedy, D., Klaveness, S., Montillo, A., Makris, N., Rosen, B., Dale, A.M.,  
 713 2002. Whole brain segmentation: automated labeling of neuroanatomical structures  
 714 in the human brain. *Neuron* 33 (2), 341–355 (Feb).
- 715 Fischl, B., van der Kouwe, A., Destrieux, C., Halgren, E., Ségonne, F., Salat, D.H., Busa, E.,  
 716 Seidman, L.J., Goldstein, J., Kennedy, D., Caviness, V., Makris, N., Rosen, B., Dale, A.M.,  
 717 2004. Automatically parcellating the human cerebral cortex. *Cereb. Cortex* 14 (3),  
 718 11–22 (Jan).
- 719 Franklin, T.R., Wang, Z., Shin, J., Jagannathan, K., Suh, J.J., Detre, J.A., O'Brien, C.P., Childress,  
 720 A.R., 2013. A VBM study demonstrating 'apparent' effects of a single dose of medica-  
 721 tion on T1-weighted MRIs. *Brain Struct. Funct.* 218 (1), 97–104.
- 722 Gernsbacher, M.A., 2007. Presidential column: the eye of the beholder. *Observer* 20 (1)  
 723 (Jan).
- 724 Gronenschild, E.H.B.M., Habets, P., Jacobs, H.I.L., Mengelers, R., Rozendaal, N., van Os, J.,  
 725 Marcelis, M., 2012. The effects of FreeSurfer version, workstation type, and Macintosh  
 726 operating system version on anatomical volume and cortical thickness measure-  
 727 ments. *PLoS ONE* 7 (6), e38234. <http://dx.doi.org/10.1371/journal.pone.0038234>.
- 728 Haier, R.J., Karama, S., Leyba, L., Jung, R.E., 2009. MRI assessment of cortical thickness and  
 729 functional activity changes in adolescent girls following three months of practice on a  
 730 visual-spatial task. *BMC Res. Notes* 2, 174. <http://dx.doi.org/10.1186/1756-0500-2-174>.
- 731 Han, X., Jovicic, J., Salat, D., van der Kouwe, A., Quinn, B., Czanner, S., Busa, E., Pacheco, J.,  
 732 Albert, M., Killiany, R., Maguire, P., Rosas, D., Makris, N., Dale, A., Dickerson, B., Fischl,  
 733 B., 2006. Reliability of MRI-derived measurements of human cerebral cortical thick-  
 734 ness: the effects of field strength, scanner upgrade and manufacturer. *Neuroimage*  
 735 32 (1), 180–194. <http://dx.doi.org/10.1016/j.neuroimage.2006.02.051> (Aug).
- 736 Hogstrom, L.J., Westlye, L.T., Walhovd, K.B., Fjell, A.M., 2013. The structure of the cerebral  
 737 cortex across adult life: age-related patterns of surface area, thickness, and  
 738 gyration. *Cereb. Cortex* 23 (11), 2521–2530. <http://dx.doi.org/10.1093/cercor/cbs231> (Nov).
- 739 Jones, S.E., Buchbinder, B.R., Aharon, I., 2000. Three-dimensional mapping of cortical  
 740 thickness using Laplace's equation. *Hum. Brain Mapp.* 11 (1), 12–32 (Sep).
- 741 Jovicic, J., Marizzoni, M., Sala-Llonch, R., Bosch, B., Bartrés-Faz, D., Arnold, J., Benninghoff, J.,  
 742 Wilfang, J., Roccatagliata, L., Nobili, F., Hensch, T., Tränkner, A., Schönenknecht, P., Leroy,  
 743 M., Lopes, R., Bordet, R., Chanoine, V., Ranjeva, J.P., Didic, M., Gros-Dagnac, H., Payoux,  
 744 P., Zoccatelli, G., Alessandrini, F., Beltramello, A., Bargalló, N., Blin, O., Frisoni, G.B., The  
 745 PharmaCog Consortium, 2013. Brain morphometry reproducibility in multi-center 3 T  
 746 MRI studies: a comparison of cross-sectional and longitudinal segmentations.  
 747 *Neuroimage*. <http://dx.doi.org/10.1016/j.neuroimage.2013.05.007> (May).
- 748 Joubault, T., Gagnon, J.F., Karama, S., Ptito, A., Lafontaine, A.L., Evans, A.C., Monchi, O., 2011. Pat-  
 749 terns of cortical thickness and surface area in early Parkinson's disease. *Neuroimage* 55  
 750 (2), 462–467. <http://dx.doi.org/10.1016/j.neuroimage.2010.12.043> (Mar).
- 751 Kim, J.S., Singh, V., Lee, J.K., Lerch, J., Ad-Dab'bagh, Y., MacDonald, D., Lee, J.M., Kim, S.I., Evans,  
 752 A.C., 2005. Automated 3-D extraction and evaluation of the inner and outer cortical sur-  
 753 faces using a Laplacian map and partial volume effect classification. *Neuroimage* 27 (1),  
 754 210–221. <http://dx.doi.org/10.1016/j.neuroimage.2005.03.036> (Aug).
- 755 Klein, A., Tourville, J., 2012. 101 labeled brain images and a consistent human cortical la-  
 756 beling protocol. *Front. Neurosci.* 6, 171. <http://dx.doi.org/10.3389/fnins.2012.00171>.
- 757 Klein, A., Ghosh, S.S., Avants, B., Yeo, B.T.T., Fischl, B., Ardekani, B., Gee, J.C., Mann, J.J.,  
 758 Parsey, R.V., 2010. Evaluation of volume-based and surface-based brain image regis-  
 759 tration methods. *Neuroimage* 51 (1), 214–220. <http://dx.doi.org/10.1016/j.neuroimage.2010.01.091> (May).
- 760 Kovacevic, J., 2006. From the editor-in-chief. *IEEE Trans. Image Process.* 15 (12).
- 761 Kuperberg, G.R., Broome, M.R., McGuire, P.K., David, A.S., Eddy, M., Ozawa, F., Goff, D.,  
 762 West, W.C., Williams, S.C.R., van der Kouwe, A.J.W., Salat, D.H., Dale, A.M., Fischl,  
 763 B., 2003. Regionally localized thinning of the cerebral cortex in schizophrenia. *Arch. Gen. Psychiatry* 60 (9), 878–888. <http://dx.doi.org/10.1001/archpsyc.60.9.878> (Sep).
- 764 Landman, B.A., Huang, A.J., Gifford, A., Vikram, D.S., Lim, I.A.L., Farrell, J.A.D., Bogovic, J.A.,  
 765 Hua, J., Chen, M., Jarso, S., Smith, S.A., Joel, S., Mori, S., Pekar, J.J., Barker, P.B., Prince,  
 766 J.L., van Zijl, P.C.M., 2011. Multi-parametric neuroimaging reproducibility: a 3-T  
 767 resource study. *Neuroimage* 54 (4), 2854–2866. <http://dx.doi.org/10.1016/j.neuroimage.2010.11.047> (Feb).
- 768 Luders, E., Narr, K.L., Thompson, P.M., Rex, D.E., Woods, R.P., Deluca, H., Jancke, L.,  
 769 Toga, A.W., 2006. Gender effects on cortical thickness and the influence of scal-  
 770 ing. *Hum. Brain Mapp.* 27 (4), 314–324. <http://dx.doi.org/10.1002/hbm.20187>  
 771 (Apr).
- 772 Luders, E., Sánchez, F.J., Tosun, D., Shattuck, D.W., Gaser, C., Vilain, E., Toga, A.W., 2012.  
 773 Increased cortical thickness in male-to-female transsexualism. *J. Behav. Brain Sci.* 2  
 774 (3), 357–362. <http://dx.doi.org/10.4236/jbbs.2012.23040> (Aug).

- 790 Lüsebrink, F., Wollrab, A., Speck, O., 2013. Cortical thickness determination of the human  
791 brain using high resolution 3 T and 7 T MRI data. *Neuroimage* 70, 122–131. <http://dx.doi.org/10.1016/j.neuroimage.2012.12.016> (Apr). 839
- 792 MacDonald, D., Kabani, N., Avis, D., Evans, A.C., 2000. Automated 3-D extraction of inner  
793 and outer surfaces of cerebral cortex from MRI. *Neuroimage* 12 (3), 340–356. 840
- 794 <http://dx.doi.org/10.1006/nimg.1999.0534> (Sep). 841
- 795 Magnotta, V.A., Andreasen, N.C., Schultz, S.K., Harris, G., Cizadlo, T., Heckel, D., Nopoulos, P.,  
796 Flaum, M., 1999. Quantitative in vivo measurement of gyration in the human  
797 brain: changes associated with aging. *Cereb. Cortex* 9 (2), 151–160 (Mar). 842
- 798 Mazziotta, J.C., Toga, A.W., Evans, A., Fox, P., Lancaster, J., 1995. A probabilistic atlas of the  
799 human brain: theory and rationale for its development. The International Consortium  
800 for Brain Mapping (ICBM). *Neuroimage* 2 (2), 89–101 (Jun). 843
- 801 Neary, D., Snowden, J., Mann, D., 2005. Frontotemporal dementia. *Lancet Neurol.* 4 (11),  
802 771–780. [http://dx.doi.org/10.1016/S1474-4422\(05\)70223-4](http://dx.doi.org/10.1016/S1474-4422(05)70223-4) (Nov). 844
- 803 Otsu, N., 1979. A threshold selection method from gray-level histograms. *IEEE Trans. Syst.  
804 Man Cybern.* 9 (1), 62–66. 845
- 805 Price, C.C., Wood, M.F., Leonard, C.M., Towler, S., Ward, J., Montijo, H., Kellison, I., Bowers, D.,  
806 Monk, T., Newcomer, J.C., Schmalzl, I., 2010. Entorhinal cortex volume in older adults:  
807 reliability and validity considerations for three published measurement protocols. *J. Int.  
808 Neuropsychol. Soc.* 16 (5), 846–855. <http://dx.doi.org/10.1017/S135561771000072X>  
809 (Sep). 849
- 810 Raji, C.A., Ho, A.J., Parikhshah, N.N., Becker, J.T., Lopez, O.L., Kuller, L.H., Hua, X., Leow, A.D.,  
811 Toga, A.W., Thompson, P.M., 2010. Brain structure and obesity. *Hum. Brain Mapp.* 31  
812 (3), 353–364. <http://dx.doi.org/10.1002/hbm.20870> (Mar). 850
- 813 Reuter, M., Schmansky, N.J., Rosas, H.D., Fischl, B., 2012. Within-subject template estimation  
814 for unbiased longitudinal image analysis. *Neuroimage* 61 (4), 1402–1418. <http://dx.doi.org/10.1016/j.neuroimage.2012.02.084> (Jul). 851
- 815 Rosas, H.D., Liu, A.K., Hersch, S., Glessner, M., Ferrante, R.J., Salat, D.H., van der  
816 Kouwe, A., Jenkins, B.G., Dale, A.M., Fischl, B., 2002. Regional and progressive  
817 thinning of the cortical ribbon in Huntington's disease. *Neurology* 58 (5),  
818 695–701 (Mar). 852
- 819 Rosas, H.D., Hevelone, N.D., Zaleta, A.K., Greve, D.N., Salat, D.H., Fischl, B., 2005. Regional  
820 cortical thinning in preclinical Huntington disease and its relationship to cognition. *Neurology*  
821 65 (5), 745–747. <http://dx.doi.org/10.1212/01.wnl.0000174432.87383.87> (Sep). 853
- 822 Salgado-Pineda, P., Delaveau, P., Falcon, C., Blin, O., 2006. Brain T1 intensity changes after  
823 levodopa administration in healthy subjects: a voxel-based morphometry study. *Br. J. Clin.  
824 Pharmacol.* 62 (5), 546–551. 854
- 825 Scott, M.L.J., Bromiley, P.A., Thacker, N.A., Hutchinson, C.E., Jackson, A., 2009. A fast,  
826 model-independent method for cerebral cortical thickness estimation using  
827 MRI. *Med. Image Anal.* 13 (2), 269–285. <http://dx.doi.org/10.1016/j.media.2008.10.006> (Apr). 855
- 828 Ségonne, F., Dale, A.M., Busa, E., Glessner, M., Salat, D., Hahn, H.K., Fischl, B., 2004. A hybrid  
829 approach to the skull stripping problem in MRI. *Neuroimage* 22 (3), 1060–1075.  
830 <http://dx.doi.org/10.1016/j.neuroimage.2004.03.032> (Jul). 856
- 831 Shattuck, D.W., Sandor-Leahy, S.R., Schaper, K.A., Rottenberg, D.A., Leahy, R.M., 2001.  
832 Magnetic resonance image tissue classification using a partial volume model.  
833 *Neuroimage* 13 (5), 856–876. <http://dx.doi.org/10.1006/nimg.2000.0730> (May). 857
- 834 Shrout, P.E., Fleiss, J.L., 1979. Intraclass correlations: uses in assessing rater reliability.  
835 *Psychol. Bull.* 86 (2), 420–428 (Mar). 858
- 836 Sled, J.G., Zijdenbos, A.P., Evans, A.C., 1998. A nonparametric method for automatic correc-  
837 tion of intensity nonuniformity in MRI data. *IEEE Trans. Med. Imaging* 17 (1), 87–97. 840
- 838 <http://dx.doi.org/10.1109/42.668698> (Feb). 841
- 839 Smith, S.M., 1996. Flexible filter neighbourhood designation. *Proc. 13th Int. Conf. on Pat-  
840 tern Recognition*, vol. 1, pp. 206–212. 842
- 841 Smith, S.M., 2002. Fast robust automated brain extraction. *Hum. Brain Mapp.* 17 (3),  
842 143–155. <http://dx.doi.org/10.1002/hbm.10062> (Nov). 843
- 843 Smith, S.M., Jenkinson, M., Woolrich, M.W., Beckmann, C.F., Behrens, T.E.J., Johansen-Berg,  
844 H., Bannister, P.R., De Luca, M., Dobbins, J., Flitney, D.E., Niazy, R.K., Saunders, J.,  
845 Vickers, J., Zhang, Y., De Stefano, N., Brady, J.M., Matthews, P.M., 2004. Advances in  
846 functional and structural MR image analysis and implementation as FSL. *Neuroimage*  
847 23 (Suppl. 1), S208–S219. <http://dx.doi.org/10.1016/j.neuroimage.2004.07.051>. 848
- 848 Talairach, J., Tournoux, P., 1988. Co-planar stereotaxic atlas of the human brain: 3-  
849 dimensional proportional system—an approach to cerebral imaging. Thieme. 850
- 850 Tustison, N.J., Avants, B.B., Cook, P.A., Zheng, Y., Egan, A., Yushkevich, P.A., Gee, J.C., 2010.  
851 N4ITK: improved N3 bias correction. *IEEE Trans. Med. Imaging* 29 (6), 1310–1320. 852
- 852 <http://dx.doi.org/10.1109/TMI.2010.2046908> (Jun). 853
- 853 Tustison, N.J., Johnson, H.J., Rohlfing, T., Klein, A., Ghosh, S.S., Ibanez, L., Avants, B., 2013.  
854 Instrumentation bias in the use and evaluation of scientific software: recommenda-  
855 tions for reproducible practices in the computational sciences. *Front. Neurosci.* 7  
856 (162). <http://dx.doi.org/10.3389/fnins.2013.00162>. 857
- 857 Vachet, C., Hazlett, H.C., Niethammer, M., Oguz, I., Cates, J., Whitaker, R., Piven, J., Styner,  
858 M., 2011. Group-wise automatic mesh-based analysis of cortical thickness. In: 859 Benoit, M., Dawant, D.R.H. (Eds.), SPIE Medical Imaging: Image Processing (February). 860
- 860 Walhovd, K.B., Storsve, A.B., Westlye, L.T., Drevon, C.A., Fjell, A.M., 2013. Blood markers of  
861 fatty acids and vitamin D, cardiovascular measures, body mass index, and physical  
862 activity relate to longitudinal cortical thinning in normal aging. *Neurobiol. Aging*. 863  
<http://dx.doi.org/10.1016/j.neurobiolaging.2013.11.011> (Nov). 864
- 864 Wang, H., Suh, J.W., Das, S.R., Pluta, J., Craige, C., Yushkevich, P.A., 2013. Multi-atlas  
865 segmentation with joint label fusion. *IEEE Trans. Pattern Anal. Mach. Intell.* 35 (1), 1–11. 866
- 866 Ward, B.D., 1999. Intracranial segmentation. Technical Report. Medical College of Wisconsin  
867 (<http://afni.nimh.nih.gov/pub/dist/doc/3dIntracranial.pdf>). 868
- 868 Wei, G., Zhang, Y., Jiang, T., Luo, J., 2011. Increased cortical thickness in sports experts: a  
869 comparison of diving players with the controls. *PLoS ONE* 6 (2), e17112. <http://dx.doi.org/10.1371/journal.pone.0017112>. 870
- 870 Wilkinson, G.N., Rogers, C.E., 1973. Symbolic description of factorial models for analysis of  
871 variance. *J. R. Stat. Soc.: Ser. C: Appl. Stat.* 22 (3), 392–399. 872
- 872 Yamasue, H., Abe, O., Kasai, K., Suga, M., Iwanami, A., Yamada, H., Tochigi, M., Ohtani, T.,  
873 Rogers, M.A., Sasaki, T., et al., 2007. Human brain structural change related to acute  
874 single exposure to sarin. *Ann. Neurol.* 61 (1), 37–46. 875
- 875 Yezzi Jr., A.J., Prince, J.L., 2003. An Eulerian PDE approach for computing tissue thickness.  
876 *IEEE Trans. Med. Imaging* 22 (10), 1332–1339. <http://dx.doi.org/10.1109/TMI.2003.817775> (Oct). 877
- 877 Zeng, X., Staib, L.H., Schultz, R.T., Duncan, J.S., 1999. Segmentation and measurement of  
878 the cortex from 3-D MR images using coupled-surfaces propagation. *IEEE Trans.  
879 Med. Imaging* 18 (10), 927–937. <http://dx.doi.org/10.1109/42.811276> (Oct). 880
- 880 Zhang, Y., Brady, M., Smith, S., 2001. Segmentation of brain MR images through a hidden  
881 Markov random field model and the expectation-maximization algorithm. *IEEE  
882 Trans. Med. Imaging* 20 (1), 45–57. <http://dx.doi.org/10.1109/42.906424> (Jan). 883
- 883